

PACS numbers: 52.80.Mg; 42.55.Lt
DOI: 10.1070/QE2011v041n03ABEH014477

Control of extended high-voltage electric discharges in atmospheric air by UV KrF-laser radiation

V.D. Zvorykin, A.O. Levchenko, N.N. Ustinovskii

Abstract. **Experiments in the commutation of extended (~ 1-m long) high-voltage (up to 390 kV) electric discharges were carried out with the aid of 100-ns long UV pulses of the GARPUN KrF laser, in which we demonstrated a one-and-a-half-fold lengthening of the discharge gap broken down in the presence of laser illumination. Total control of discharge trajectory along the direction of the laser beam was observed for a radiation energy of ~300 mJ (the corresponding intensity $I = 5\times10^8$ W cm^{-2} and its attendant initial electron density $N_e \sim 10^{11}$ cm^{-3}) and partial control for an energy of 40 mJ ($I = 7\times10^7$ W cm^{-2}, $N_e \sim 8\times10^9$ cm^{-3}) with a 100% probability of breakdown. We discuss the advantages of employing a UV laser for active lightning protection in comparison with IR lasers and ultrashort-pulse laser systems.**

Keywords: *electric breakdown, UV laser illumination, active lightning protection.*

1. Laser-assisted production of electroconductive channels in the air

Laser-assisted production of extended electroconductive plasma channels in the atmospheric air is of interest for the initiation of high-voltage discharges (in particular, for active lightning protection [1,2]), for the wireless transmission of electric power and current pulses, as well as for reducing the divergence of electromagnetic radiation of the radio frequency and microwave ranges by means of transmitting plasma antennas or artificial plasma waveguides [3–5]. In early experiments in the initiation of high-voltage electric discharges, use was made of pulsed Nd (with a wavelength λ = 1.06 μm) and CO_2 lasers (λ = 10.6 μm) [6–8]. An optical breakdown of gas emerged in the focused laser beams for the respective intensities of ~10^{10} and ~10^8 W cm^{-2}, in which the avalanche ionisation of the gas was caused by inverse bremsstrahlung [9]. The multiphoton ionisation of atomic oxygen with an ionisation potential I_i = 12.06 eV and nitrogen with I_i = 15.58 eV for the low photon energy $h\nu$ = 1.17 eV of Nd-laser radiation is unlikely and plays some part only at an early stage of electron avalanche development. For a CO_2 laser with $h\nu$ = 0.117 eV, the multiphoton ionisation is at all negligible, and the seed electrons in the avalanche arise from the natural background ionisation of the air or by the vaporisation and ionisation of aerosol particles. The plasma length is determined by the propagation of the plasma front along the laser beam caustic due to different hydrodynamic or radiative transfer mechanisms in the so-called absorption wave or breakdown wave [9,10]. The absorption wave front travels with a velocity of 10^3–10^4 m s^{-1}, depending on the radiation intensity and the propagation regime, in the opposite direction to the laser pulse, and the length of the optical breakdown plasma does not exceed ~10 cm in the course of the laser pulse, 0.1 μs–1 ms. In the breakdown wave, the avalanche ionisation front propagates with a high phase velocity along the caustic of the laser beam as the intensity of the laser pulse builds up. The length of this long laser-induced spark (LLIS) ranges up to several metres; however, as a rule it consists of separate stochastic plasma sites. The longer the caustic waist of the focused laser beam and the smaller the excess of the intensity over the gas breakdown threshold intensity, the greater the separation between these sites. Because of the inhomogeneous structure of the LLIS, the electric resistance of its channel is high, which hinders the breakdown of the gap to which the voltage is applied. In this case, there occurs a lowering of the breakdown threshold due to plasma polarisation and the intensification of the electric field between separate plasma sites, although a certain role is played by the photoionisation of gas by the intrinsic UV plasma radiation.

In order to form a continuous LLIS in a gas, the laser radiation is focused with an axicon – a conical lens or mirror [11]. Unlike spherical optics, the axicon concentrates the radiation along a lengthy axial segment, affording the beam convergence along the cone generator at an angle γ to the axicon's axis. The length of the focal segment $L_a = R/\gamma$, where R is the radius of the axicon, increases with decreasing γ; however, this is attended with an increase in the transverse diameter $d = 2.4/(\pi\gamma)$ of the focal region, with the consequential lowering of the on-axis radiation intensity. The side feed of the radiation to different points located along the focal segment of the axicon obviates the effect of plasma screening [12]. Although the axicon's focal segment may theoretically be very long (over 100 m), the length of the continuous plasma channel in the air obtained in actual laboratory experiments with the employment of CO_2 and Nd lasers did not exceed ~1.5 m and involved high expenditures of energy (~200 J m^{-1}) for the production of dense optical breakdown plasmas [13,14].

Numerous laboratory experiments in the initiation of high-voltage electric discharges facilitated by laser-induced sparks (see, for instance, a topical journal issue [15]) have promoted endeavours to control lightnings with a laser. In field experiments [16] it has been possible to record several events of lightning initiation with the help of a 2-m long LLIS, which

V.D. Zvorykin, A.O. Levchenko, N.N. Ustinovskii P.N. Lebedev Physics Institute, Russian Academy of Sciences, Leninsky prosp. 53, 119991 Moscow, Russia; Advanced Energy Technologies Ltd, ul. Neglinnaya 14, 107031 Moscow, Russia;
e-mail: zvorykin@sci.lebedev.ru

Received 29 October 2010
Kvantovaya Elektronika **41** (3) 227–233 (2011)
Translated by E.N. Ragozin

was directed towards a thundercloud from the top of a 50-m high tower. It is significant that in addition to two high-power CO_2 lasers (with an energy of ~1 kJ and a pulse duration of ~50 ns each) and an Nd laser (600 J, 50 ns), the long path directed to the thundercloud was illuminated with a train of low-energy (~100 mJ) UV pulses (λ = 264 nm) of the fourth harmonic of Nd-laser radiation, which followed at a repetition rate of 70 Hz.

According to Refs [1, 2], lightning control is expected to be most effective in the initiation of a downward leader stroke from the lower edge of a thundercloud. To do this requires producing and maintaining with a laser for ~10 μs a ~20-m long conductive channel with an electron density $N_e \sim 10^{12}$ cm^{-3} at an altitude of at least 1 km. The flow of electric charge along this channel will result in its polarisation and a strengthening of the electric field at its ends. The multiphoton gas ionisation by the UV radiation of excimer lasers or by the third/fourth harmonic of solid-state laser radiation allows producing lengthy plasma channels in a subthreshold regime, since the optical breakdown thresholds of the air are significantly higher, namely ~10^{11} W cm^{-2} [17–23]. For instance, three KrF-laser radiation photons ($h\nu$ = 5 eV) are sufficient to produce one free electron in the photoionisation of oxygen. In this case, the temperature of heavy particles in the nonequilibrium plasma will be significantly lower than the electron temperature $T_e \sim 1$ eV and the degree of ionisation will be many orders of magnitude lower than in the avalanche air breakdown ($N_e \sim 10^{19}$ cm^{-3}), and the expenditures of laser energy will be accordingly lower. However, even when the breakdown threshold is exceeded, the electron density in a singly ionised air plasma $N_e = 2.7\times10^{19}$ cm^{-3} will be two orders of magnitude lower than the critical density $N_{e\,cr} = \pi c^2 m_e/(e^2\lambda^2) = 1.6\times10^{22}$ cm^{-3} for the radiation with λ = 248 nm, with the consequence that this plasma will remain transparent for the incident radiation.

New possibilities opened up with the use of ultrashort laser pulses (USPs) of femtosecond duration with multiterawatt peak power. When propagating through the atmosphere, bandwidth-limited USPs (having the minimum short duration for a given spectral bandwidth) broaden in time due to dispersion of the refractive index of the air. However, by introducing negative phase modulation (chirping) of the radiation frequency into the initial pulse it is possible to compensate its spreading and obtain the temporal compression of the USP as it propagates through the atmosphere. When the peak power of the USP exceeds the critical power $P_{cr} = 3.77\lambda_0^2/(8\pi n_0 n_2)$ (λ_0 is the radiation wavelength in vacuum, n_0 and n_2 are the linear and nonlinear parts of the refractive index $n = n_0 + n_2 I$, and I is the intensity), the laser beam disintegrates into ionised filamentary channels (filaments) with a characteristic diameter of ~100 μm and an electron density of 10^{16}–10^{17} cm^{-3}, which transmit the radiation with an intensity of 10^{13}–10^{14} W cm^{-2} in the very-low-loss self-consistent regime (see, for instance, Refs [24–27]). The greatest length L of a filaments-initiated electric discharge in laboratory experiments involving a titanium-sapphire laser (with a central wavelength λ = 790 nm, peak USP power of 200 TW, and a USP duration of 150 fs) was equal to ~4 m for a voltage $U \sim 2$ MW across the discharge gap [28–40]. The effect of filaments on electric discharges in a thundercloud was observed in field experiments [41].

Since the free-electron lifetime $\tau_e \sim 10$ ns in an air plasma is limited by electron attachment to O_2 molecules or by electron–ion recombination (for $N_e \geqslant 10^{14}$ cm^{-3}), the electron conduction produced by a USP persists over a relatively small filament length $l_e = c\tau_e \sim 3$ m, which approximately coincides with the maximum controllable discharge length L obtained in experiments. To increase the length L ($L \gg l_e$) calls for maintaining ionisation for a substantially longer time required for the development of electric breakdown. Such a maintenance may be carried out by subsequent long pulses ($\tau_{las} \gg \tau_e$) of the visible or UV range by way of photodetachment of electrons from the negatively charged molecular ions O_2^-, which is possible for a substantially lower intensity than the multiphoton ionisation of the gas induced by a USP [19, 20, 41–44]. For an electron binding (affinity) energy in O_2^- ($\varepsilon \sim 0.5$ eV), the threshold wavelength for electron photodetachment is $\lambda \approx 2.5$ μm. Despite this, the cross section of this process in the UV range exceeds the threshold value by two orders of magnitude [45]. Note that in the experiments of Ref. [21] a controllable high-voltage discharge of length L = 34 cm for a voltage U = 260 kV was initiated by KrF-laser radiation with an energy E_{las} = 750 mJ and a pulse duration τ_{las} = 21 ns, which is only slightly longer than the free-electron lifetime.

In the present work, lengthy (~1 m) high-voltage (U = 390 kV) discharges in the atmospheric air were initiated by long (~100 ns) high-power (~1 GW) KrF-laser radiation pulses, which produced and maintained the ionisation of the air for a relatively long time $\tau_{las} \gg \tau_e$. We investigated the feasibility of controlling the discharge with lower radiation intensity (energy) and under different polarities of the voltage across the discharge gap.

2. Initiation of lengthy discharges by the GARPUN KrF laser

Experiments in high-voltage discharge initiation are schematised in Fig. 1. The e-beam pumped GARPUN KrF laser operated in the regime involving injection of the seed radiation of the master oscillator into an unstable resonator [46]. The maximum output laser energy ranged up to 100 J for a FWHM pulse duration τ_{las} = 75 ns. The laser beam had a quasistationary angular intensity distribution with a divergence of 0.1–0.15 mrad and was focused into the discharge gap with a long-focus lens with F = 8 m. The focal beam waist was $d \sim 1$ mm and the caustic length measured ~10 cm. For an output laser energy $E_{las} \geqslant 25$ J (which corresponded to a

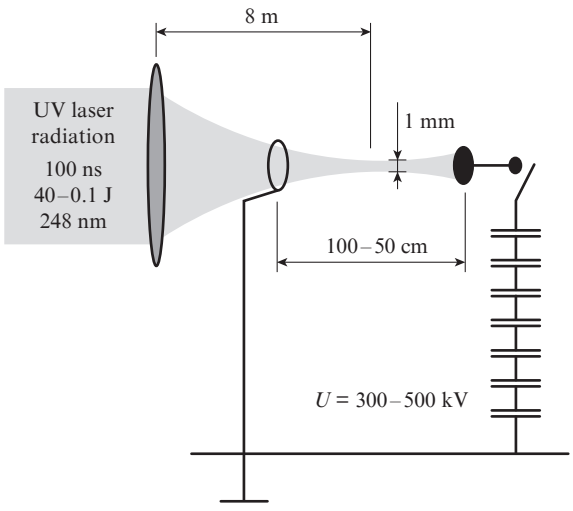

Figure 1. Schematic representation of experiments in high-voltage discharge initiation.

radiation intensity $I = E_{las}/[\tau_{las}(\pi d^2/4)] \sim 4\times10^{10}$ W cm^{-2}, in the vicinity of the lens focus there emerged an optical air breakdown in the form several plasma sites. For lower energies (to this end, limiting apertures were mounted at the laser output or the pump energy was lowered), optical breakdown was absent.

The radiation was introduced into the discharge gap through an 18-mm diameter opening in a grounded electrode fabricated in the form of a hemisphere 75 mm in diameter (Fig. 2). To smooth out the spatial distribution of the electric field, it was surrounded with a polished aluminium ring 250 mm in diameter. The high-voltage electrode was a hemisphere 30 mm in diameter mounted on the end of cylindrical rod. The lens focus was at a distance of $L/2$ to $L/3$ from the high-voltage electrode for a gap length $L = 50-80$ cm. Smaller L values corresponded to self-breakdown of the gap, and larger values corresponded to the maximum length of controllable discharge for an applied voltage $U = 390$ kV. The voltage pulse was generated by a seven-stage Marx pulse voltage generator (PVG) assembled of IK-100-0.25 capacitors. The shock capacitance of the PVG was equal to 0.036 μF and the voltage amplitude ranged from 300 to 500 kV. The voltage pulse shape was measured with a low-inductance shunt with a resistance of ~2 kΩ and the current in the discharge circuit was measured with a Rogowski coil.

a

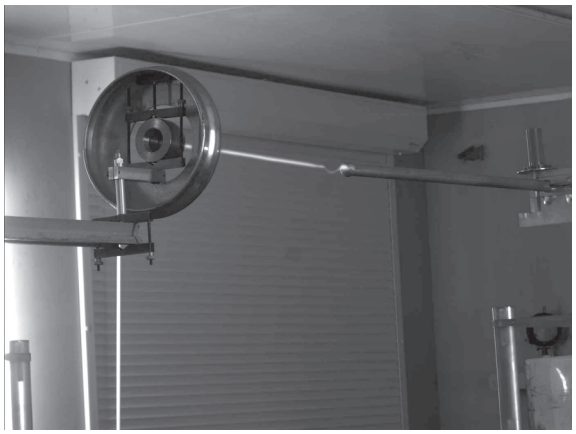

b

Figure 2. Images of discharge gap and discharge in the regimes of self-breakdown (a) and breakdown controlled by UV laser radiation (b). The interelectrode distance is equal to 60 cm.

Figure 2 shows the photographs of the discharge gap and electric discharge in the self-breakdown and laser-controlled regimes, which were obtained with a Videoscan-285 digital video camera. Since the glow intensity of the discharge was many times higher than illumination intensity in the laboratory room, its images were recorded with the use of neutral-density filters with a total optical density $D = 5.6$ (the corresponding attenuation was equal to 0.25×10^{-5}). The images of the discharge were next superimposed, using a computer, with the photograph of the gap and the electrodes recorded without the light filters. For a voltage pulse amplitude $U = 390$ kV, the self-breakdown of the gap of length $L \leqslant 50$ cm occurred with a nearly 100% probability and developed along a stochastic trajectory. For $L = 60$ cm, self-breakdown was unlikely to occur, while under UV laser illumination it occurred with a ~100% probability and coincided exactly with the direction of laser beam propagation. For $L \geqslant 80$ cm, the breakdown probability for the indicated voltage became low even in the presence of laser illumination.

Figure 3 shows typical oscilloscope traces of a laser pulse, discharge current in the case of discharge commutation, and the voltage applied to the gap (without discharge commutation). The voltage pulse in the absence of gap breakdown exhibits a rise time of ~0.3-μs and a ~4.5-μs long descending part, which is defined by the draining of the charge of the PVG via its own charging resistors. The laser pulse arrives at the discharge gap ~2 μs after the peak of the voltage pulse, when the voltage decreases by about 20%. The breakdown of the gap and the current through it emerged with some delay τ, which depended on the voltage amplitude U, its polarity, the gap length L, and the laser pulse energy E_{las}.

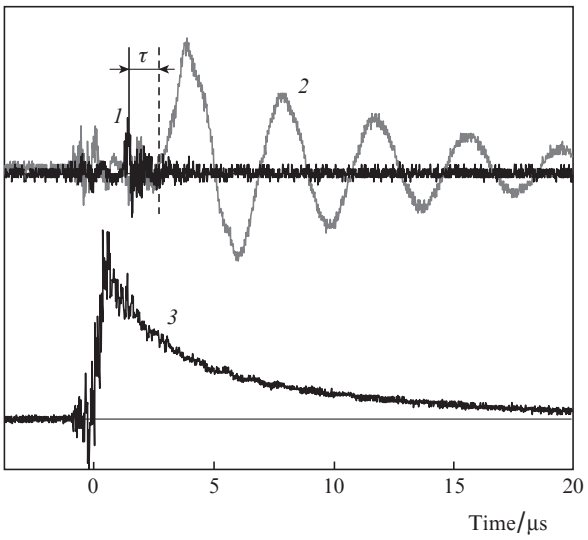

Figure 3. Oscilloscope traces of a laser pulse (*1*), discharge current (*2*), and the voltage across the gap without discharge commutation (*3*).

The discharge current has a damping oscillatory shape and is described by the formula

$$i(t) = A_0 \exp\left(-\frac{R_c}{2L_c}t\right) \times\left[\frac{R_c}{2L_c}\sin(\omega t + \alpha_0) - \omega\cos(\omega t + \alpha_0)\right], \quad (1)$$

where the oscillation frequency

$$\omega = \sqrt{\frac{1}{L_c C} - \frac{R_c^2}{4L_c^2}},$$

the initial amplitude

$$A_0 = CU\left(1 - \frac{R_c^2 C}{4L_c}\right)^{-1/2},$$

and the amplitude decay time $\tau_{dec} = 2L_c/R_c$.

On the commutation the PVG voltage had the same shape but was shifted by $\pi/2$ in phase. From the measured values of the period $T = 4$ μs and decay time $\tau_{dec} = 4.5$ μs, for the known PVG capacitance $C = 0.036$ μF it is possible to find the inductance L_c and resistance R_c of the discharge circuit. To take into account the contribution made by the resistance of the PVG's spark gaps to the total resistance of the discharge circuit, we performed current and voltage measurements when the discharge gap was short-circuited by a copper conductor with a large cross section (20 mm^2) and a negligible intrinsic resistance. Experiments for a gap length $L = 60$ cm showed that the total inductance of the discharge circuit was independent of the way of short-circuiting the gap and was equal to 10 μH. On short-circuiting the gap with a copper conductor, the total circuit resistance $R_c = 1.6$ Ω, for a laser-controlled gap breakdown $R_c = 1.8–2.2$ Ω, and for a self-breakdown without laser illumination $R_c = 2.2–2.3$ Ω. Therefore, the intrinsic resistance of the laser-controlled plasma column $R_{las} = 0.2–0.4$ Ω, while for a self-breakdown it is only slightly higher: 0.4–0.5 Ω, which is evidently attributable to the greater length of the stochastic channel.

Figure 4 shows the delays τ of the onset of discharge current relative to the arrival of the laser pulse at the discharge channel as functions of the radiation energy E_{las} for different voltage polarities. For $E_{las} \geqslant 10$ J the delay does not exceed 0.1 μs irrespective of the polarity of the voltage applied. The delay increases with decreasing energy, this increase being stronger for the positive polarity of the voltage at the high-voltage electrode. The threshold of controllable breakdown $E_{las}^{th} \approx 40$ mJ, which corresponds a laser radiation intensity in the beams waist $I \sim 7\times10^7$ W cm^{-2}. Note that the lengthening of delay to 5 μs resulted in a decrease of the voltage to 30% of the maximum value (see Fig. 3), which was supposedly the reason why the gap breakdown did not occur for energies $E_{las} \leqslant E_{las}^{th}$ and accordingly for longer delays.

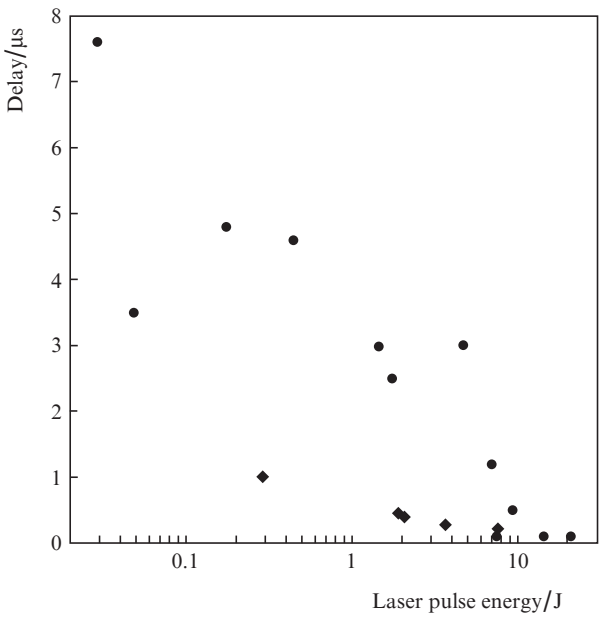

Figure 4. Delay of discharge current relative to the laser pulse for positive (●) and negative (◆) voltage polarities.

The change of discharge character (trajectory) with a decrease in laser pulse energy E_{las} may be traced in Fig. 5. In the absence of voltage across the electrodes and for $E_{las} \geqslant 25$ J we observed (in the laser beam waist near the lens focus) separate faintly glowing regions of optical breakdown as well as the glow of the electrode which the laser radiation was incident on (Fig. 5b). On application of a voltage pulse of positive polarity with an amplitude $U = 390$ kV, the maximum controllable discharge length $L = 80$ cm (Fig. 5c). On lowering the energy, the length of controllable part of discharge (coinciding with the laser beam caustic) became shorter, the rectilinear portion persisting in a limited domain of the focal region (Figs 5d and 5e) where the intensity of laser radiation was highest. For $E_{las} \leqslant E_{las}^{th} = 40$ mJ the discharge trajectory became random (Fig. 5f). We emphasize that without UV laser illumination the gap of length $L = 60$ cm with a high probability did not break down at all. For a negative polarity of the voltage at the high-voltage electrode (Fig. 5g), the discharge was effectively directed along all the entire length of the discharge gap even for a relatively low energy of laser radiation $E_{las} \sim 0.3$ J ($I \sim 5\times10^8$ W cm^{-2}), at which only an incomplete discharge control was observed in the case of positive polarity.

3. Typical values of electron density produced by UV laser illumination

In earlier experiments [4] (see also Ref. [47]), from photoconductivity measurements we found the quasistationary photoelectron density produced by the 22-ns long pulses of UV KrF-laser radiation in the atmospheric air (Fig. 6). The laser radiation with an energy of 5–200 mJ varied by means of attenuators was focused by lenses with focal lengths $F = 0.5$ or 2 m into the gap between two hollow tubular electrodes (to eliminate the photoeffect from electrode surfaces). The interelectrode distance (several millimetres) was so selected as to be approximately equal to the length of the focal region, so that the intensity of laser radiation remained approximately the same throughout the length of the discharge gap. The lateral intensity distribution was measured with a profilometre. The average FWHM diameter of the focal spot was measured at ~100 μm for the lens with a focal length $F = 2$ m. For the other lens, the distribution shape was similar and the spot diameter was proportional to its focal length. In all, by lowering the pulse energy, changing the focal length of the lens, and, in addition, defocusing the laser beam (by transferring the lens focus beyond the discharge gap), in our experiments it was possible to vary the intensity in the range between 3×10^6 and 7×10^{10} W cm^{-2}. To determine the density from the measured conductivity, use was made of electron mobility $\mu_e \sim 10^3$ cm^2 V^{-1} s^{-1} in the discharge gap [1]. Preliminarily we verified that the photocurrent as a function of voltage and interelectrode gap obeyed Ohm's law.

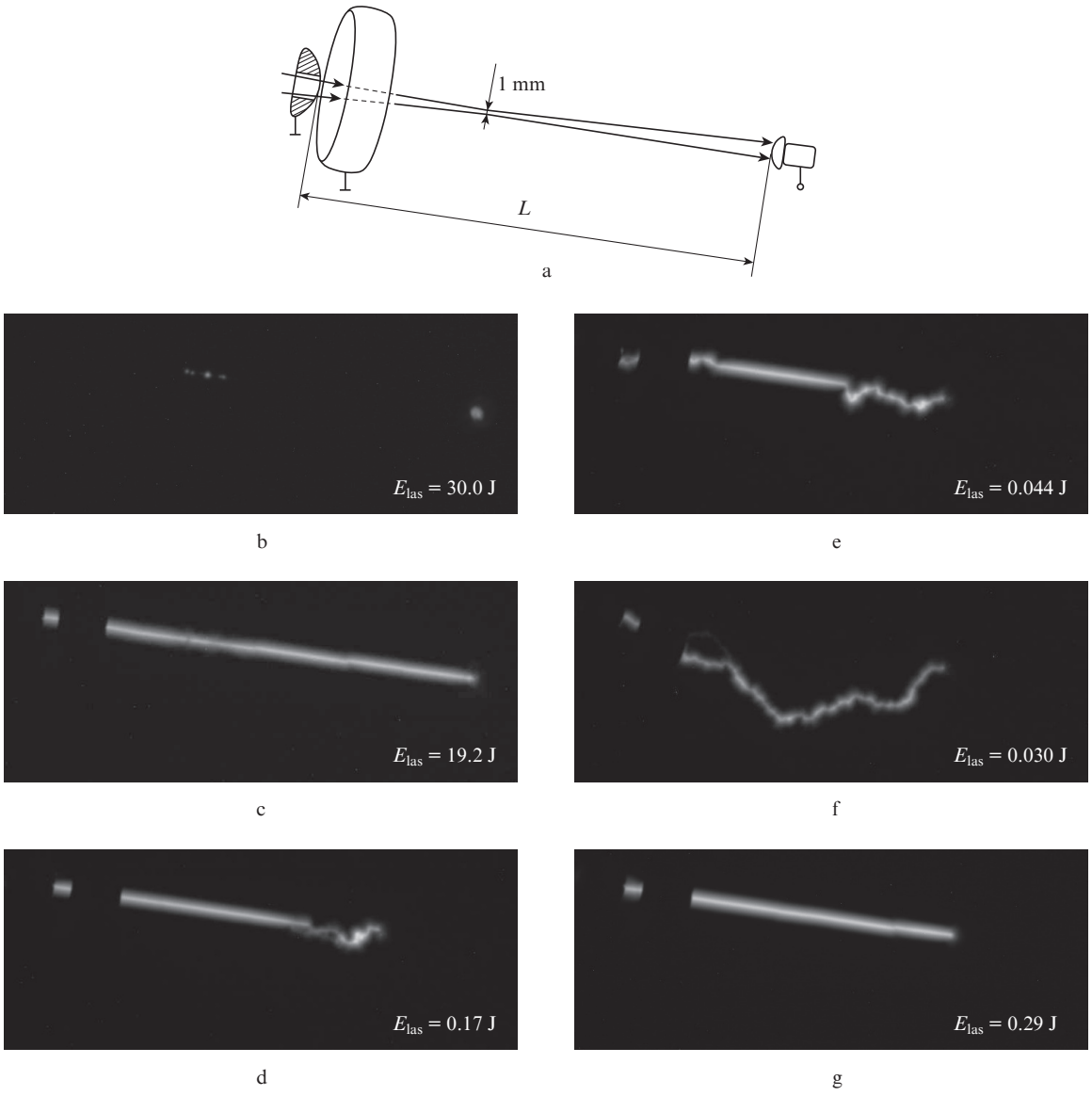

Figure 5. Schematic representation (a) and photographs of the discharge gap for interelectrode distances L = 80 (b, c) and 60 cm (d–g) in the absence (b) and in the presence of positive (c–f) and negative (g) voltage U = 390 kV for different laser pulse energies E_{las}.

In Fig. 6 there are two domains which differ by the character of the intensity (I) dependence of the electron density N_e. For relatively high intensities $I = 3\times10^8 - 7\times10^{10}$ W cm^{-2} (yet below the optical air breakdown threshold of $\sim10^{11}$ W cm^{-2}) this dependence is of the form $N_e \sim I^2$, which is typical for the two-stage process involving two-photon excitation of oxygen to an intermediate state with subsequent rapid single-photon ionisation. Observed in the low-intensity domain (3×10^6–3×10^8 W cm^{-2}) was a linear dependence $N_e \sim I$, which is attributable to the two-stage single-photon ionisation of complex organic impurity molecules with low ionisation potentials via intermediate resonance levels. Since the UV photon energies exceed the work function for the majority of materials, the photoeffect on aerosol microparticles is not ruled out, either.

Also shown for comparison in Fig. 6 are the dependences calculated for direct three-photon ionisation of the air for different cross sections $\sigma^{(3)}$. It is pertinent to note that the values of $\sigma^{(3)}$ given in different papers for oxygen were either calculated by the Keldysh formula or determined experimentally, their values diverging by three orders of magnitude (ranging from 1.9×10^{-28} to 3×10^{-31} cm^6 s^2 J^{-3}). One can see that in any case the three-photon ionisation was insignificant.

A more reliable interpretation calls for additional investigations into the photoionisation of the air and its main components, electron–ion recombination, and the electron photodetachment from electronegative O_2^- ions. However, the characteristic initial values of the electron density in the initiation of electric breakdown may be found from the $N_e(I)$ dependence at hand (Fig. 6). In particular, to the controllable-breakdown threshold ($I = 7\times10^7$ W cm^{-2}) there corresponds $N_e \sim 8\times10^9$ cm^{-3}, and to the intensity $I = 5\times10^8$ W cm^{-2}, at which we observed complete control of discharge, there corresponds $N_e \sim 10^{11}$ cm^{-3}.

4. Conclusions

In experiments in the commutation of lengthy (~1-m long) high-voltage (up to 390 keV) electric discharges by 100-ns

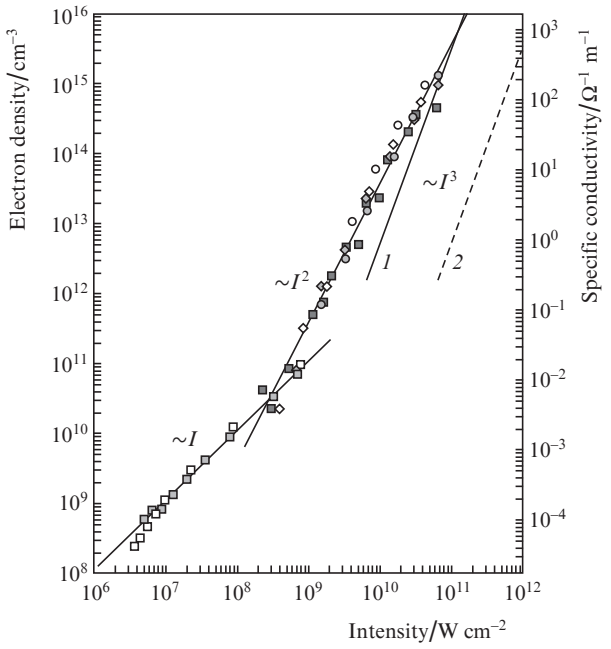

Figure 6. Electron density and specific plasma conductivity as functions of intensity in different series of experiments involving variations of the focal length of the lens, the voltage, and the length of the interelectrode gap. Curves (*1*) and (*2*) represent calculations for the direct three-photon ionisation of oxygen for cross sections $\sigma^{(3)} = 1.9\times10^{-28}$ (*1*) and 3×10^{-31} cm^6 s^2 J^{-3} (*2*).

long UV KrF-laser pulses we demonstrated a one-and-a-half-fold lengthening of the discharge gap broken down in the presence of laser illumination. Total control of discharge trajectory along the direction of the laser beam was observed for a radiation energy of ~300 mJ (the corresponding intensity $I = 5\times10^8$ W cm^{-2} and its attendant initial electron density $N_e \sim 10^{11}$ cm^{-3}); discharge initiation with a probability close to 100%, under partial control (in the focal region of the lens) took place even for 40 mJ ($I = 7\times10^7$ W cm^{-2}, $N_e \sim 8\times10^9$ cm^{-3}). The UV radiation energy required to initiate electric discharge and control it, therefore, was three orders of magnitude lower than for IR lasers (CO_2 and Nd lasers) for similar pulse lengths and turned out to be comparable with the energy of the high-intensity USPs ($\tau_{las} \leqslant 100$ fs) of the titanium-sapphire laser employed for the same purposes. Unlike USP-induced ionisation, which is attended with the filamentation of the laser beam and a rapid electron relaxation in a time of ~10 ns, the lengthy high-voltage discharge in our experiments was initiated due to the ionisation of the air by the UV radiation of relatively low intensity $I = 10^8$–10^9 W cm^{-2}; the UV radiation maintained the requisite electron density during the course of the laser pulse (~100 ns), which exceeded the electron relaxation time by an order of magnitude. The advantage of this discharge initiation regime is the relative simplicity of the laser system, and so this regime is a candidate for the development of an active lightning protection technology.

Acknowledgements. The authors are grateful to I.V. Smetanin for discussions of experimental results.

This work was supported by the Russian Foundation for Basic Research (Grant No. 09-07-13593-ofi_ts). One of the authors (A.O. Levchenko) expresses his appreciation to the LPI Educational-Scientific Complex for support.

References

1. Baselyan E.M., Raizer Yu.P. *Fizika molnii i molniezashchita* (The Physics of Lightning and Lightning Protection) (Moscow: Fizmatlit, 2001).
2. Baselyan E.M., Raizer Yu.P. *Usp. Fiz. Nauk*, **170** (7), 753 (2000) [*Phys.-Usp*, **43** (7), 701 (2000)].
3. Askar'yan G.A. *Zh. Eksp. Teor. Fiz.*, **55**, 1400 (1968).
4. Zvorykin V.D., Levchenko A.O., Molchanov A.G., et al. *Kratk. Soobshch. Fiz.*, (2), 49 (2010).
5. Zvorykin V.D., Levchenko A.O., Smetanin I.V., Ustinovskii N.N. *Pis'ma Zh. Eksp. Teor. Fiz.*, **91**, 244 (2010).
6. Koopman D.V., Wilkenson T.D. *J. Appl. Phys.*, **42**, 1883 (1971).
7. Greig J.R., Koopman D.W., Fernsler R.F., et al. *Phys. Rev. Lett.*, **41**, 174 (1978).
8. Zvorykin V.D., Nikolaev F.A., Kholin I.V., et al. *Fiz. Plazmy*, **5**, 1140 (1979).
9. Raizer Yu.P. *Lazernaya iskra i rasprostranenie razryadov* (Laser Spark and Discharge Propagation) (Moscow: Nauka, 1974).
10. Danilychev V.A., Zvorykin V.D. *Tr. Fiz. Inst. Akad. Nauk SSSR*, **142**, 117 (1983).
11. Korobkin V.V., Marin M.Yu., Pil'skii V.I., et al. *Kvantovaya Elektron.*, **12**, 959 (1985) [*Sov. J. Quantum Electron.*, **15**, 631 (1985)].
12. Pyatnitskii L.N., Korobkin V.V. *Tr. Inst. Obshchei Fiz. Ross. Akad. Nauk*, **57**, 59 (2000).
13. Bychkov S.S., Marin M.Yu., Pyatnitskii L.N. *Tr. Inst. Obshchei Fiz. Ross. Akad. Nauk*, **50**, 166 (1995).
14. Apollonov V.V., Vasilyak L.M., Kazantsev S.Yu., et al. *Kvantovaya Elektron.*, **32**, 115 (2002) [*Quantum Electron.*, **32**, 115 (2002)].
15. Upravlenie razryadom molnii s pomoshch'yu lazernogo izlucheniya (Lightning Discharge Control with the Aid of Laser Radiation) *Opt. Zh.*, **66** (3) (1999).
16. Uchida S., Shimada E., Yasuda H., et al. *Opticheskii Zh.*, **66** (3), 36 (1999).
17. Antipov A.A., Grasyuk A.Z., Zhigalkin A.K., et al. *Zh. Tekh. Fiz.*, **61**, 200 (1991).
18. Losev L.L., Soskov V.I. *Pis'ma Zh. Tekh. Fiz.*, **18**, 76 (1992).
19. Zhao X.M., Diels J.-C. *Laser Focus World*, **29**, 113 (1993).
20. Zhao X.M., Wang Y.C., Diels J.-C., Elizondo J. *IEEE J. Quantum Electron.*, **31**, 599 (1995).
21. Miki M., Wada A. *J. Appl. Phys.*, **80**, 3208 (1996).
22. Rambo P., Biegert J., Kubicek V., et al. *Opt. Zh.*, **66** (3), 30 (1999).
23. Rambo P., Schwarz J., Diels J.-C. *J. Opt. A: Pure Appl. Opt.*, **3**, 146 (2001).
24. Rodriguez M., Bourayon R., Mejean G., et al. *Phys. Rev. E*, **69**, 036607 (2004).
25. Mechain G., Mejean G., Ackermann R., et al. *Appl. Phys. B*, **80**, 785 (2005).
26. Berge L., Skupin S., Nuter R., et al. *Rep. Progr. Phys.*, **70**, 1633 (2007).
27. Couairon A., Mysyrowicz A. *Phys. Rep.*, **441** (2-4), 47 (2007).
28. La Fontaine B., Vidal F., Comtois D., et al. *IEEE Trans. Plasma Sci.*, **27**, 688 (1999).
29. Vidal F., Comtois D., Chien C.Y., et al. *IEEE Trans. Plasma Sci.*, **28**, 418 (2000).
30. Desparois A., La Fontaine B., Bondiou-Clergerie A., et al. *IEEE Trans. Plasma Sci.*, **28**, 1755 (2000).
31. Comtois D., Chien C.Y., Desparois A., et al. *Appl. Phys. Lett.*, **76**, 819 (2000).
32. Pepin H., Comtois D., Vidal F., et al. *Phys. Plasmas*, **8** (5), 2532 (2001).
33. Rodriguez M., Saurbrey R., Wille H., et al. *Opt. Lett.*, **27**, 772 (2002).
34. Comtois D., Pepin H., Vidal F., et al. *IEEE Trans. Plasma Sci.*, **31**, 377 (2003).
35. Comtois D., Pepin H., Vidal F., et al. *IEEE Trans. Plasma Sci.*, **31**, 387 (2003).
36. Gordon D.F., Ting A., Hubbard R.F., et al. *Phys. Plasmas*, **10**, 4530 (2003).
37. Ackerman R., Mechain G., Mejean G., et al. *Appl. Phys. B*, **82**, 561 (2006).

38. Houard A., D'Amico C., Liu Y., et al. *Appl. Phys. Lett*., **90**, 171501 (2007).
39. Aleksandrov N.L., Baselyan E.M., Bogatov N.A., et al. *Fiz. Plazmy*, **34**, 1142 (2008).
40. Fujii T., Miki M., Goto N., et al. *Phys. Plasmas*, **15**, 013107 (2008).
41. Kasparian J., Ackermann R., Andre Y.-B., et al. *Opt. Express*, **16**, 5757 (2008).
42. Hao Z.Q., Zhang J., Li Y.T., et al. *Appl. Phys. B*, **80**, 627 (2005).
43. Mejean G., Ackerman R., Kasparian J., et al. *Appl. Phys. Lett.*, **88**, 021101 (2006).
44. Narayanan V., Singh V., Pandey P.K., et al. *J. Appl. Phys.*, **101**, 073301 (2007).
45. Burch D.S., Smith S.J., Branscomb L.M. *Phys. Rev.*, **112**, 171 (1958).
46. Basov N.G., Vadkovskii A.D., Zvorykin V.D., et al. *Kvantovaya Elektron*., **21**, 15 (1994) [*Quantum Electron.*, **24**, 13 (1994)].
47. Zvorykin V.D., Ionin A.A., Kudryashov S.I., et al. *Proc. 51th Workshop of the INFN ELOISOTRON Project «Charged and Neutral Particle Channeling Phenomena».* Ed. by S.B. Dabagov, L. Palumbo (New Jersey–London–Singapore: World Scientific, the Science and Culture Ser.-Physics, 2008) p. 813.